Journal of Physics: Conference Series

PAPER • **OPEN ACCESS**

Computational modelling of cervix radiation procedure using a virtual anthropomorphic phantom and the MCNPX code

To cite this article: William S. Santos *et al* 2021 *J. Phys.: Conf. Ser.* **1826** 012040

View the article online for updates and enhancements.

This content was downloaded from IP address 143.107.255.190 on 03/06/2021 at 19:47

Computational modelling of cervix radiation procedure using a virtual anthropomorphic phantom and the MCNPX code

William S. Santos [a,b,*], Lucio P. Neves [a,c], Ana P. Perini [a,c], Carla J. Santos [c], Walmir Belinato [d], Rogerio M. V. Silva [e], Maria R. Soares [f], Caio C. Valeriano [g], Linda V. E. Caldas [b]

[a] Instituto de Física, Universidade Federal de Uberlândia (INFIS/UFU), Uberlândia, MG, Brazil.

[b] Instituto de Pesquisas Energéticas e Nucleares, Comissão Nacional de Energia Nuclear (IPEN-CNEN/SP), São Paulo, SP, Brazil.

[c] Programa de Pós-Graduação em Engenharia Biomédica, Faculdade de Engenharia Elétrica, Universidade Federal de Uberlândia, Uberlândia, MG, Brazil.

[d] Instituto Federal da Bahia (IFBA), Vitória da Conquista, BA, Brazil.

[e] Hospital Haroldo Juçaba, Fortaleza, CE, Brazil.

[f] Fundação Universidade Federal de Rondônia (UNIR), Porto Velho, RO, Brazil.

[g] Programa de Pós-Graduação em Educação, Universidade Tiradentes, Aracaju, SE, Brazil.

*william@ufu.br

Abstract. There is a serious, and growing concern about the increased risk of the emergence of a secondary cancer, radio-induced, associated with radiotherapy treatments. To assess the radiation doses to organs outside the target volume, in this work, several computational exposure scenarios were modelled, based on Monte Carlo simulation (MCNPX code). A Varian 2100c accelerator, and a female virtual anthropomorphic phantom were used, in a simulated treatment of cervical cancer. The determination of the dispersed dose would be important for assessing the risk in different organs or tissues. Four treatment fields were applied, varying the gantry angle. It was possible to observe that the conversion factors for equivalent dose were higher for the AP projection. For the RLAT and LLAT projections, the results were similar, fact that may be attributed to the symmetrical distributions of the organs in relation to the radiation source. The results presented in this work showed that the computational exposure scenario provides a versatile and accurate tool to estimate in a ready way the absorbed doses during a cervical treatment.
Keywords: Dosimetry, radiotherapy, Monte Carlo simulation, MCNPX, anthropomorphic phantom

Content from this work may be used under the terms of the Creative Commons Attribution 3.0 licence. Any further distribution of this work must maintain attribution to the author(s) and the title of the work, journal citation and DOI.
Published under licence by IOP Publishing Ltd

1. Introduction

According to Bray *et al.* [1] the cervix cancer is the sixth most common cancer type in women worldwide. This type of tumor is the third most frequent among the women population, behind the breast and colorectal cancer. It occupies the fourth place in the cause of women death [2]. With the diagnosis of cervical cancer, treatment options vary, and depending on the stage external radiotherapy may be indicated. Despite the treatment efficiency, radiotherapy may cause injuries at patients, since healthy tissues located closer, or inside, the treated area are exposed to the photon beam. These effects are characterized as acute effects, such as erythema or a late effect such as a secondary tumor. As presented in several works in the literature [3 - 8], the determination of the dispersed dose would be important for assessing the risk and biological consequences in different organs or tissues. This subject is of great concern, mainly when new treatment techniques may increase the leakage radiation to patients.

The absorbed doses to organs and tissues outside the radiation planning field are unavoidable during the treatment, and may contribute to the induction of a secondary cancer. These doses are derived from the scattered radiation throughout the patient's body, walls, floor and ceiling of the radiotherapy room, head, collimators and other structures of the LINAC [9].

Most studies found in the literature are focused on the determination of absorbed dose distributions inside the treatment planned area [10,11]. These works aimed the modelling of the main components of the beam line, such as the target, primary collimator, jaws, and the flattening filter. The presence of the patient, which is more important to scattered radiation, was not considered.

The Monte Carlo (MC) simulation has been widely used to model primary treatment fields of various LINAC models, such as Varian, Siemens and Elekta [4]. To determine the doses in different organs and tissues, the Monte Carlo simulation is used coupled with virtual anthropomorphic phantoms. The aim of this study is to estimate the absorbed doses in tissues and organs located outside the volume of the radiotherapeutic planning. In this study the 2D planning mode was considered for cervix cancer. For this, a computational model was developed using Monte Carlo simulation coupled with the computational anthropomorphic phantom (FASH3), representing the patient, and a Varian 2100c LINAC. The results are presented in the format of conversion factors (CF).

2. Material and Methods

2.1. Computational model description

In this work the MCNPX software (version 2.7.0) [12] was used to model the scenario with a medical Varian 2100c LINAC. The photon and electron transport were carried out based on the ENDF/B-VI8 cross section libraries, with a cutoff energy of 0.01MeV for photons, and 0.1MeV for electrons. The photon transport was considered including photoelectric absorption with the possibility of fluorescent emission and Auger electron, coherent and incoherent scattering. The Varian 2100c LINAC, using a 6 MV photon beam, was modelled with the target, wedge filter, jaws and a detailed 80 leaf multi-leaf collimator (MLC) [5,6]. The primary and secondary collimators, as well as other structures that may affect the leakage and scattering radiation were also considered. The validation was obtained comparing the simulated results with those obtained experimentally.

An 8×8×3 m³ radiotherapy room with walls and concrete ceiling (2.43 g/cm³ density) with 1 m thickness was modeled, as well as the extra slabs for primary radiation shielding. In addition, the floor has 20 cm thick concrete. Besides the equipment, the room was filled with atmospheric air (0.001205 g/cm³ density). Figure 1 presents the computational scenario with the adult phantom on the positioning table, the gantry of the LINAC, the positioning table made of carbon fiber, with 10 cm thickness, 17 cm wide and 200 cm length, supported by a metallic base. The adult patient was represented by a female virtual anthropomorphic phantom, developed at the Federal University of Pernambuco (UFPE – Brazil) [13]. This phantom has 60 kg of body mass and 1.63 m of height and is composed of more than a hundred organs and tissues with dosimetric importance. It was formed with voxels of dimensions 2.4×2.4×2.4 cm³, each one. To avoid unnecessary exposure of the patient's arms

and, consequently, higher doses in the red bone marrow (RBM) and bone surface (BS), as performed in a real treatment, the arms of this phantom were removed.

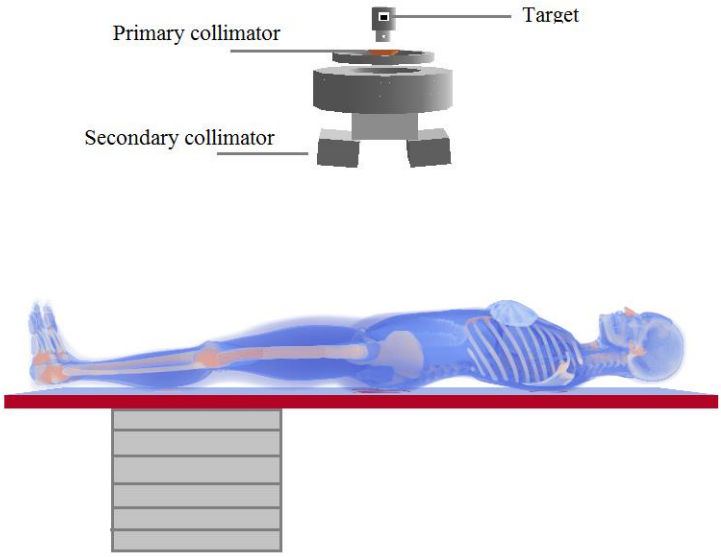

Figure 1. Computational model employed in this work for the radiotherapy procedure.

During the treatment, four treatment fields were applied. The radiation field was directed to the cervix. The treatment fields, and gantry angles, were: 16×16 cm^2 (projections antero-posterior (AP/0°) and postero-anterior (PA/180°) and 16×12 cm^2 (projections right lateral (RLAT/90°) and left lateral (LLAT/270º). The MCNP mesh tally was used to determine the photon fluence profile and to test the beam collimation, with the LINAC operating at 6 MV with the MLC.

2.2. Scenario validation

The validation of the beam properties was done by means of comparisons of the percentage depth dose (PDD) and dose profiles (Off-axis), calculated with the results of experimental measurements. The PDD results were simulated at various depths within a water phantom, using the tally *F8 (MeV/particle-source) to evaluate the energy deposited in the water, along the central axis of the field.

To determine the PDD and the Off-axis, it was necessary to model a set of voxels to represent the radiation detectors. The first set consists of 400 voxels distributed along the central axis and the second set with 100 voxels along the axial axis. The energy deposited in each voxel of the central and the axial axes were used to determine the PDD and Off-axis, respectively. For the determination of the PDD, voxels with dimensions 2.5×2.5×0.1 cm^3 were used, and for Off-axis calculations 1.0×1.0×0.4 cm^3 voxels were used. The PDD calculations were made with the detectors spaced 1 mm apart, and during experimental measurements, they were spaced 0.5 cm apart.

A Gaussian spatial distribution was chosen for the electron source, along the *xy* axis, with a half height width (FWHM) of 0.13 cm. The PDD and Off-axis simulations were performed using a PMMA phantom of dimensions 40×40×40 cm^3 filled with water. The phantom has an open top and 1 cm thick PMMA on its sides.

The Varian 2100c LINAC was operated (experimentally) with a voltage of 6 MV and the photon beam irradiating a field of 10×10 cm^2 with a source-surface distance (SSD) of 100 cm. Figure 2 shows the computational model used to determine the dose profile (Off-axis) and PDD.

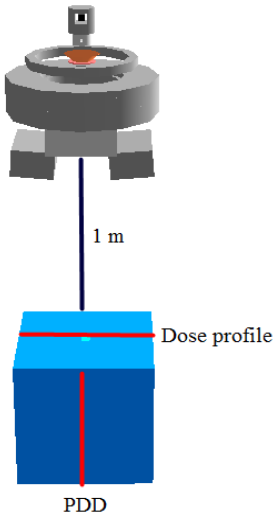

Figure 2: Computational model used in determination of the PDD and Off-axis ratio.

The PDD and Off-axis measurements were performed using a Farmer ionization chamber (model FC65/P – IBA dosimetry) with a sensitive volume of 0.6 cm^3. The PDD was measured with the ionization chamber positioned along the central axis with depths ranging from 0.5 to 30 cm in 0.5 cm steps. The Off-axis was measured along the axial axis with 0.025 cm steps. PDD and Off-axis were normalized by the absorbed dose at 10 cm depth on the central axis.

2.3. Dosimetric calculations

A set of absorbed doses in organs and tissue located inside, or in the proximity, of the target area during cervix radiotherapy, for an adult patient, were determined. The dosimetric results were due to the scattered primary photons and secondary electrons. The absolute dose of a set of organs and tissues with dosimetric importance, recommended by the International Commission on Radiological Protection [14], were calculated using Equation 1. The assumed prescribed treatment delivered 45 Gy to the target area of the cervix. This amount was divided into 28 fractions, where each day 1.8 fractions were delivered. The treatment took 25 days, divided in 5 days groups in a row, as normally carried out in these treatments.

$$D(Gy) = \frac{D_T}{D_C} x D_P \quad (1)$$

where D_T is the estimated absorbed dose in each organ or tissue T, D_C is the dose in the cervix volume and D_P is the total dose prescribed for all radiotherapy treatment. In this study, the ratio $\frac{D_T}{D_C}$ is determined as the conversion factor (CF).

The dose deposition was determined using the tally F6:p (MeV/g/source-particle), which could be converted into Gy, for all organs and tissues, except for the red bone marrow (RBM), where the tally ∗F4 (MeV/cm^2/particle) was used. For all simulations, to determine the organ doses 5.0E8 particles histories were used. To assess the beam properties (PDD, Off-axis and photon fluence) 1.0E9 particles histories were used, providing results with less than 2% uncertainty.

3. Material and Methods

3.1. Dosimetric properties of the simulated radiation beam

Figure 3 shows the comparison between the PDD curves calculated with the MCNPX and those measured with the ionization chamber, at various depths in the water phantom, for a field size of

10×10 cm². The results were normalized to a dose corresponding to a depth of 10 cm (d_{10}), a region of more stability than d_{max}. The difference between the experimental and simulated results is within ±2%.

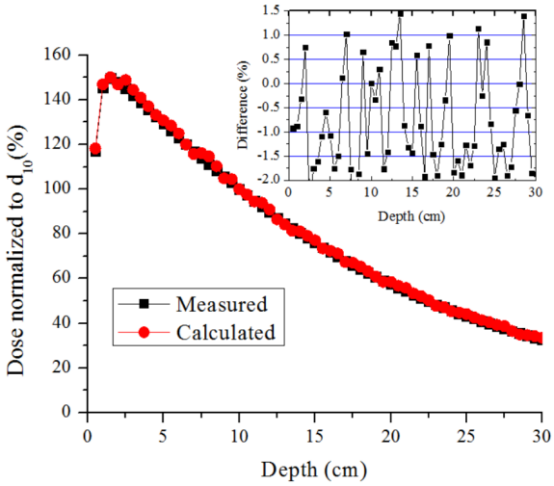

Figure 3. Measured and calculated (MCNPX) PDD for a Varian 2100c with 6 MV beam.

The lateral profiles, measured and calculated, at a depth of 10 cm, are shown in Figure 4. It is noted that the distances of the detectors decrease with respect to the center of the beam. The simulated Off-axis is slightly overestimated in the region between -5 cm and -2.5 cm and 2.5 cm and 5 cm. These differences (< 4%) between the simulated and experimental results are attributed to the small volume of the detectors, immersed in the water phantom. However, this does not affect the quality of the results. In the overall set of results, the Off-axis ratio is practically uniform in the field of 10×10 cm², showing that the geometry of the flattening filter and the modelled collimators are correct. In the regions near the edge, the calculated and experimental results presented differences of less than 2%.

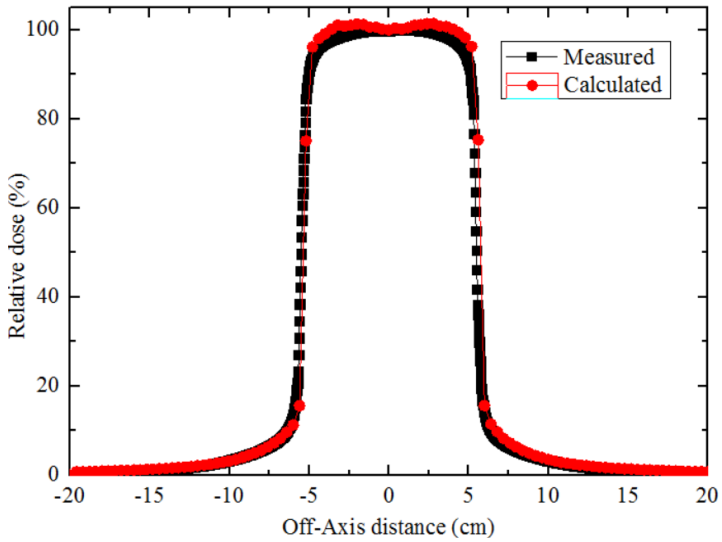

Figure 4. Measured and calculated (MCNPX) lateral profile – Varian 2100c LINAC with 6 MV beam and 10×10 cm² field.

Besides the dose profile, the beam collimation, for the 16×16 cm² (AP/PA) and 16×12 cm² (RLAT/LLAT) reference fields with the MLC were also evaluated. In this part of the work, the mesh tally MCNPX command was utilized. This command allowed the creation of the photon fluence maps

for the four projections studied in this work. In Figure 5, it is possible to view that the radiation field margins with MLC are properly delimited, confirming the correct collimation.

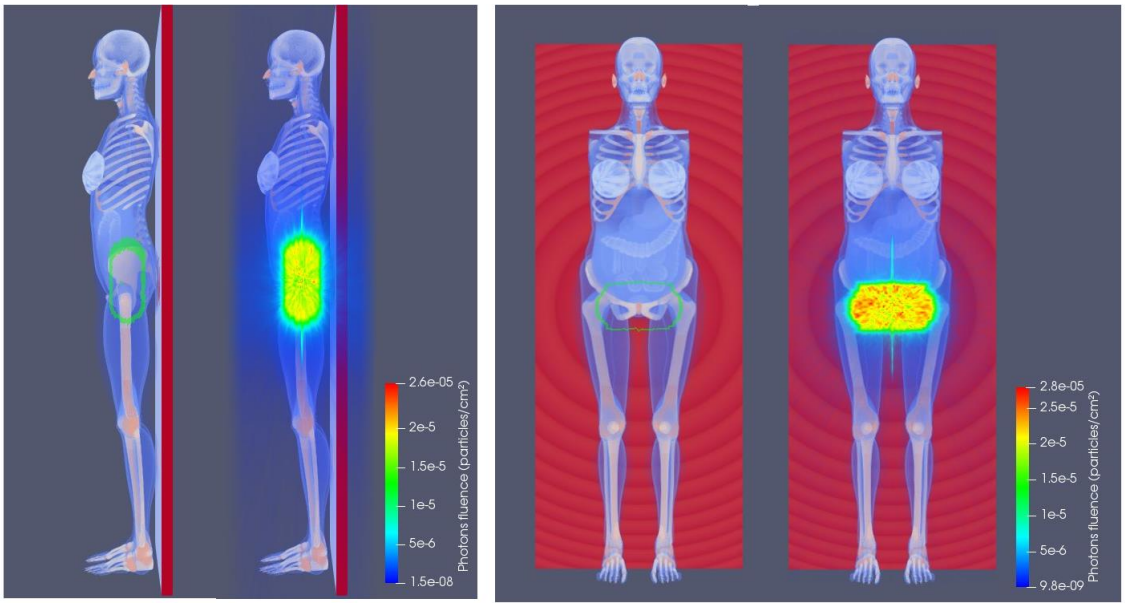

(a) (b)

Figure 5. Photon fluence maps (particles/cm^2): View of the beam collimation for right lateral projection RLAT (a) and antero-posterior AP projection (b) of the treated region of the FASH3 anthropomorphic phantom.

3.2. Dosimetric results

The CF values were calculated, as a function of the gantry angle, for absorbed doses of a set of organs and tissues located inside and outside the treatment region. The results of these factors by projection, and the absorbed dose of the complete treatment, are shown in Table 1. Using the mean CF value, by projection of each organ, the absolute absorbed dose was determined for the major organs/tissues, as suggested by the ICRP 103 [14].

It is possible to observe that the highest dose values were obtained for organs located near, or within, the irradiated volume (cervix), such as large intestine (colon), small intestine, gonads and bladder. The doses calculated for the bladder (44.3 Gy) and gonads (45.6 Gy), which are within the irradiated area, received a dose similar to the prescribed dose of the cervix (45 Gy).

Another important fact is that for the same field size (AP/PA), the results of the CF values for AP/0° projection, were mostly higher than for the PA/180° projection. In these cases, the gantry is under the table, which may shield the low energy photons. The spine of the patient may also shield these photons, reducing the dose for the organs located in this region. For the RLAT/90º and LLAT/270º projections, the CF values were mostly similar, fact that can be attributed to the symmetrical distributions of the organs in relation to the radiation source. For the same irradiation conditions, the skin and the bone surface, which are evenly distributed throughout the human body, the differences in CF values were small, i.e., they do not depend on the irradiation position.

In addition to these differences, it is important to note that the breasts, organs located superficially and distant from the target organ, obtained an average absorbed dose of 0.30 Gy, which is a value close to the mean value calculated for the heart (0.29 Gy). This fact can be associated with the contribution of scattered radiation from the collimators and the leakage radiation of the LINAC head. The organs

relatively distant from the non-targeted ones presented the lowest CF values, since they received just the scattered radiation.

The percentage relative uncertainty of each organ and tissue estimated by the MCNPX code is presented between parentheses. The eye and eyes lenses have relatively small volumes and, therefore, the statistical uncertainties of these organs were the largest, and they varied between 7% and 27%. For all other organs and tissues, in all evaluated situations, the uncertainties in the CF values were below 4%.

Table 1. CF values for absorbed doses per beam projection for a treatment using a 2D planning system. The relative uncertainties of the simulations are shown in parentheses.

	Conversion Factor (CF)				**Average**
Organs and tissues	**AP**	**LLAT**	**PA**	**RLAT**	**dose (Gy)**
Bone marrow	2.55E-02 (0.3%)	5.26E-02 (0.4%)	2.67E-02 (0.3%)	5.94E-02 (0.4%)	1.85E+00
Colon	2.52E-01 (0.1%)	2.93E-01 (0.2%)	2.74E-01 (0.1%)	2.89E-01 (0.2%)	1.25E+01
Lung	6.46E-03 (0.4%)	5.63E-03 (0.6%)	6.76E-03 (0.4%)	5.53E-03 (0.6%)	2.74E-01
Stomach	2.36E-02 (0.5%)	1.63E-02 (0.8%)	1.92E-02 (0.5%)	1.66E-02 (0.8%)	8.51E-01
Breast	9.05E-03 (0.6%)	6.03E-03 (1.0%)	5.69E-03 (0.7%)	6.14E-03 (1.0%)	3.03E-01
Remainder tissues	1.80E-02 (0.0%)	2.37E-02 (0.1%)	1.60E-02 (0.1%)	2.29E-02 (0.1%)	9.07E-01
Gonads	1.08E+00 (0.3%)	1.03E+00 (0.5%)	8.92E-01 (0.3%)	1.05E+00 (0.4%)	4.56E+01
Bladder	1.14E+00 (0.2%)	9.12E-01 (0.3%)	9.07E-01 (0.2%)	9.85E-01 (0.3%)	4.43E+01
Oesophagus	5.84E-03 (1.5%)	5.44E-03 (2.1%)	5.62E-03 (1.3%)	5.48E-03 (2.3%)	2.52E-01
Liver	2.09E-02 (0.4%)	1.16E-02 (0.6%)	1.73E-02 (0.4%)	1.17E-02 (0.6%)	6.93E-01
Thyroid	4.81E-03 (2.6%)	2.87E-03 (4.1%)	2.54E-03 (3.3%)	2.53E-03 (4.0%)	1.43E-01
Bone surface	1.26E-01 (0.1%)	1.89E-01 (0.1%)	1.03E-01 (0.1%)	1.91E-01 (0.1%)	6.85E+00
Brain	1.66E-03 (1.1%)	1.87E-03 (1.3%)	1.23E-03 (1.3%)	1.89E-03 (1.3%)	7.48E-02
Salivary glands	3.72E-03 (1.7%)	2.63E-03 (2.2%)	1.68E-03 (2.3%)	2.63E-03 (2.1%)	1.20E-01
Skin	9.01E-02 (0.1%)	7.55E-02 (0.1%)	6.94E-02 (0.1%)	7.77E-02 (0.1%)	3.52E+00
Uterus	1.00E+00 (0.2%)	1.00E+00 (0.2%)	1.00E+00 (0.2%)	1.00E+00 (0.2%)	4.50E+01
Heart	7.26E-03 (0.9%)	5.99E-03 (1.2%)	6.44E-03 (0.8%)	5.88E-03 (1.2%)	2.88E-01
Thymus	6.71E-03 (2.3%)	4.59E-03 (3.3%)	4.40E-03 (1.8%)	4.67E-03 (3.4%)	2.29E-01
Pancreas	5.33E-02 (0.5%)	2.32E-02 (1.0%)	4.25E-02 (0.5%)	2.35E-02 (1.0%)	1.60E+00
Spleen	1.49E-02 (1.0%)	1.40E-02 (1.1%)	1.36E-02 (1.0%)	1.36E-02 (1.1%)	6.30E-01
Lymphatic nodes	1.65E-01 (0.1%)	1.90E-01 (0.2%)	1.19E-01 (0.1%)	2.33E-01 (0.2%)	7.95E+00
Adrenals	1.60E-02 (1.8%)	1.20E-02 (2.3%)	1.57E-02 (1.6%)	1.19E-02 (2.3%)	6.25E-01
Gall bladder	4.57E-02 (1.0%)	1.74E-02 (1.5%)	3.25E-02 (1.0%)	1.79E-02 (1.6%)	1.28E+00
Extra-thoracic region	3.69E-03 (2.5%)	2.20E-03 (4.2%)	1.68E-03 (3.5%)	2.28E-03 (4.0%)	1.11E-01
Kidneys	2.31E-02 (0.5%)	1.74E-02 (0.8%)	2.35E-02 (0.4%)	1.67E-02 (0.9%)	9.09E-01
Oral mucosa	3.27E-03 (2.2%)	2.56E-03 (2.8%)	1.35E-03 (2.8%)	2.68E-03 (2.9%)	1.11E-01
Small intestine	2.91E-01 (0.1%)	2.39E-01 (0.2%)	1.97E-01 (0.1%)	3.12E-01 (0.2%)	1.17E+01
Muscle	1.62E-02 (0.0%)	2.21E-02 (0.1%)	1.47E-02 (0.1%)	2.09E-02 (0.1%)	8.31E-01
Eyes	3.03E-03 (3.3%)	2.05E-03 (4.8%)	8.79E-04 (6.5%)	2.15E-03 (6.0%)	9.12E-02
Eye lens	3.08E-03 (8.8%)	2.09E-03 (16%)	1.09E-03 (27%)	1.79E-03 (14%)	9.05E-02

4. Conclusions

The gantry angles considerably affected the results. The majority of the organs near or inside the target volume were those that received the highest radiation doses. Regarding the influence of the gantry angle, the higher CF values were obtained for the AP/0º projection. Usually, the absorbed dose of the organs depends on the location, distribution of the organs in the body and the distance of the treated volume. Comparing the dose values with the prescribed value for the cervix, the organs and tissues outside the treated region that received the highest doses were the large intestine (28%), small intestine (26%), the lymph nodes and the bone surface (15%).

During the treatment, it is impossible to measure experimentally the doses due to the scattered radiation within the patient's body. Therefore, the CF values calculated in this study will be useful to readily estimate the absorbed doses during a cervix treatment. Besides the traditional analytical planning systems, the computational modelling presented in this study may be an alternative tool for dosimetry calculations.

Acknowledgements
The authors would like to thank Dr. Richard Kramer for kindly providing the virtual anthropomorphic phantoms used in this work. This work was partially supported by the Brazilian agencies: Fundação de Amparo à Pesquisa do Estado de Minas Gerais (FAPEMIG, Grants No. APQ-03049-15 and APQ-02934-15), Conselho Nacional de Desenvolvimento Científico e Tecnológico (CNPq Grants No. 421603/2016-0, 420699/2016-3 and 301335/2026-8) and Fundação de Amparo à Pesquisa do Estado de São Paulo (FAPESP, Grant No. 2018/05982-0).

References

[1] Bray F, Soerjomataram I, Siegel RL, Torre LA, Jemal A. Global cancer statistics 2018: GLOBOCAN estimates of incidence and mortality worldwide for 36 cancers in 185 countries. CA Cancer J Clin. 68, p.394–424, 2018.
[2] INCA. Instituto Nacional do Câncer. Estimativa de casos de câncer em homens e mulheres entre 2010 e 2014. (Estimates of cancer cases in men and women between 2010 and 2014), 2018. Accessed in 26/06/2018: http:www.inca.gov.br.
[3] Xu XG, Bednarz B, Paganetti H. A review of clinical data and radiation dosimetry methods on secondary cancers from external beam radiation treatments. Phys. Med. Biol. 53, p. 193- 241, 2008.
[4] Bednarz B, Xu XG. A feasibility study to calculate unshielded fetal doses to pregnant patients in 6-MV photon treatments using Monte Carlo methods and anatomically realistic phantoms. Med Phys. 35, p. 3054 - 61, 2008.
[5] Brenner DJ, Curtis RE, Hall EJ, Ron E. Second malignancies in prostate carcinoma patients after radiotherapy compared with surgery. Cancer, 88, p. 398 - 406, 2000.
[6] Hall E, Wu CS. Radiation-induced second cancers: the impact of 3D-CRT and IMRT. Int. J. Radiat. Oncol. Biol. Phys. 56, p. 83-88, 2003.
[7] Mesbahi A, Seyednejad F, Gasemi-Jangjoo A. Estimation of organs doses and radiation-induced secondary cancer risk from scattered photons for conventional radiation therapy of nasopharynx: a Monte Carlo study. Jpn. J. Radiol. 28, p. 398-403, 2010.
[8] Kry SF, Salehpour M, Followill DS, Stovall M, Kuban DA, White RA, et al. Out-of-field photon and neutron dose equivalents from step-and-shoot intensity-modulated radiation therapy. Int. J. Radiat. Oncol. Biol. Phys. 62, p.1204-1216, 2005.
[9] Taylor ML, Kron T. Consideration of the radiation dose delivered away from the treatment field to patients in radiotherapy. J. Med. Phys. 36, 59-71, 2011.
[10] Verhaegen F, Seuntjens J. Monte Carlo modelling of external radiotherapy photon beams. Phys. Med. Biol. 48, p. 107-164, 2003.
[11] Rijkee AG, Zoetelief J, Raaijmakers CPJ, Van DMSC and Van DZW. Assessment of induction of secondary tumours due to various radiotherapy modalities. Radiat. Prot. Dosim. 118, p. 219-226, 2006.
[12] Pelowitz D B. MCNPX User`s Manual, Version 2.7.0. Report LA-CP-11-00438. Los Alamos National Laboratory, 2008.
[13] Cassola V F, de Lima V J, Kramer R, Khoury H J. FASH and MASH: Female and male adult human phantoms based on polygon mesh surfaces. Part II. Dosimetric calculations. Phy. Med. Biol. 55, p. 163-189, 2010.
[14] ICRP 103. International Commission on Radiological Protection. Recommendations of the ICRP publication 103. Elsevier, 37, p. 61-62, 2007.